https://doi.org/10.5194/gmd-2022-314
Preprint. Discussion started: 22 March 2023

Geoscientific Model Development
Discussions

G&M3D 1.0: an Interactive framework for 3D Model Construction and Forward Calculation of Potential Fields

Kanggui Wei[1,2], Bo Chen[1,3,4], Jiaxiang Peng[1]

[1] School of Geosciences and Info-Physics, Central South University, Changsha 410083, China
[2] School of Electronic, Electrical and Communication Engineering, University of Chinese Academy of Sciences, Beijing 100049, China
[3] Hunan Key Laboratory of Non-ferrous Resources and Geological Hazard Detection, Changsha 410083, China
[4] Key Laboratory of Metallogenic Prediction of Nonferrous Metals and Geological Environment Monitoring (Central South University), Ministry of Education, Changsha 410083, China

Correspondence to: Bo Chen (bochen@csu.edu.cn)

Abstract. Building source models and performing forward calculations are the basis for data processing, analysis, and interpretation of geophysical data. However, open-source tools for flexibly constructing source models and forward modelling of the potential fields are still lacking. This paper developed a new MATLAB-based software — G&M3D 1.0 to fill this gap. The software has two main functions: (1) constructing 3-D gravity and magnetic source models and (2) calculating and visualizing their gravity and magnetic fields. In the 3D-Modeling Module, rectangular prisms are used to approximate anomalous geologic bodies. Users can flexibly construct 3-D regular-shaped models with variable densities or magnetic parameters using the Sphere, Cylinder, and Cube tools, or build irregular-shaped models using the Irregular (Layer-Building) tool. On the other hand, the gravity anomalies, gravity gradients, total magnetic intensity, and magnetic gradients generated by the created 3-D sources can be rapidly calculated, visualized, and saved in the Forward-Modelling Module of G&M3D 1.0. In order to improve the efficiency of the gravity and magnetic forward calculations, the 2-D discrete convolution algorithm is improved and applied in the software for the forward modelling of the gravity and magnetic fields. Finally, we use G&M3D 1.0 for the forward gravity modelling over a salt dome in Vinton Dome, southern Louisiana, U.S., which verifies its correctness and practicality.

1 Introduction

As the most conventional geophysical exploration methods, gravity and magnetic explorations have the advantages of simple construction, low cost, and efficient large-area data acquisition compared with other exploration methods. Building forward source models and carrying out forward calculations are the basis for data processing, analysis, and interpretation of gravity and magnetic data (Blakely, 1996). However, open-source tools for flexibly constructing source models and forward modelling of the potential fields are still lacking.

In order to estimate the gravitational or magnetic effects generated by anomalous masses, the complex subsurface volume or geological bodies are commonly built by a sum of idealized sources with simple shapes (Blakely, 1996; Hinze et al., 2013),

https://doi.org/10.5194/gmd-2022-314
Preprint. Discussion started: 22 March 2023

Geoscientific Model Development Discussions

such as spheres, cylinders, vertical laminas, horizontal laminas, prisms, and polyhedron. Most of these idealized sources can be readily integrated by volume and evaluated in closed analytical forms. Among these simple cells, the rectangular prism has been favoured for forward modelling and inversion since it provides a straightforward way to approximate a complicated anomalous source and the total underground volume without holes (Caratori Tontini et al., 2009; Li and Chouteau, 1998; Zhao et al., 2018).

Many early scholars have contributed to the closed formulas of gravity and magnetic anomalies due to rectangular prisms (Bhattacharyya, 1964; Bhattacharyya and Navolio, 1976; Li and Chouteau, 1998; Nagy, 1966; Nagy et al., 2000; Okabe, 1979; Plouff, 1976). For example, Bhattacharyya (1964) gave the formulas for the magnetic anomalies due to prism-shaped bodies with arbitrary polarization. Nagy (1966) derived a closed expression for calculating the gravitational attraction of a rectangular prism. Bhattacharyya and Navolio (1976) provided the spectrum expressions of the gravity and magnetic anomalies due to irregular 3-D sources by combining prisms. Guo et al. (2004) gave a new singularity-free calculation formula for the forward modelling of the magnetic field of a rectangular prism. Luo and Yao (2007) optimized the theoretical magnetic calculation formula to improve its calculation efficiency.

A fine subdivision is often required to approximate anomalous bodies more precisely. However, when the subspace is finely subdivided, the repeated cumulative calculation makes the forward analysis time-consuming. In order to improve the calculation efficiency, various algorithms have been developed for forward calculations of gravity and magnetic anomalies. For example, Wu and Tian (2014) proposed a Gauss-fast Fourier transform (FFT) method for calculating potential fields in the Fourier domain. Zhang and Wong (2015) created a block-Toeplitz-Toeplitz-block (BTTB) structure through a discrete multi-layer model and then embedded the BTTB matrix into the block-cyclic-cyclic-block (BCCB) matrix by using FFT in the forward calculation. On the other hand, Chen and Liu (2019) optimized the computation of the weight coefficient matrix and applied a 2-D discrete convolution algorithm by block circulant extension (named BCE method) in calculating gravity anomaly in the spatial domain. This method was also extended to calculate magnetic anomalies on undulating terrain (Qiang et al., 2019). Subsequently, Hogue et al. (2020) developed an open-source MATLAB code for evaluating gravity and magnetic kernel based on the BCE method. Recently, Yuan et al. (2022) developed the BCE algorithm for magnetic forward modelling and inversion.

Although significant progress has been achieved in the forward calculation of the potential fields, constructing a 3-D anomalous model that is used to test forward or inversion algorithms is usually not intuitive and cumbersome, especially building some complex irregular sources (Jessell et al., 2021). Various packages exist for the computational synthesis of different geological models (de la Varga et al., 2019; Hassanzadeh et al., 2022; Jessell et al., 2014; Jessell et al., 2021; Pirot et al., 2022; Wellmann et al., 2016). However, open-source software in which we can interactively create geologic bodies and perform efficient forward calculations of their potential fields is rare. This study aims to develop free, open-source software that combines flexible model construction and fast-forward calculations of the potential fields.

As a scientific computing tool, MATLAB has excellent advantages in matrix computing and is widely used in geophysical research. At the same time, the GUI, APP Designer, and other toolkits launched by MATLAB have made it popular in software

https://doi.org/10.5194/gmd-2022-314
Preprint. Discussion started: 22 March 2023

development. For example, the software Potensoft (Özgü Arısoy and Dikmen, 2011) and gTools (Battaglia et al., 2022) have been developed for gravity and magnetic data processing. In addition, MATLAB is applied in developing codes for gravity and magnetic inversion (Pallero et al., 2021; Pham et al., 2020; Stocco et al., 2009).

In this study, we chose the rectangular prism as the primary cell to approximate the source volume. Then we developed a software named G&M3D 1.0 for constructing 3-D density and magnetic susceptibility models, and forward calculating and visualizing their gravity and magnetic fields based on the APP Designer platform of MATLAB. The software includes the following functions: (1) interactively creating various geological models and assigning density contrasts or magnetization parameters; (2) performing fast and accurate forward calculations of gravity, gravity gradients, total magnetic intensity, and magnetic gradients. In addition, the models built by G&M3D 1.0 can be visualized and saved, and their density or magnetization distributions can be exported. Also, the forward modelling results can be flexibly visualized and saved.

The paper is organized as follows. Section 2 introduces the principle of gravity, magnetic forward calculation, and fast calculation strategies. In section 3, we show the workflow of the software, mainly describing how to create a source model and conduct forward modelling. Section 4 is an example of applying G&M3D 1.0 to the real-world forward gravity modelling in Vinton Dome, southern Louisiana, U.S. The last section is the conclusions.

2 Forward Method

2.1 Forward modelling theory

As shown in Fig. 1, a collection of rectangular prisms provided a simple way to approximate a mass volume (Li and Chouteau, 1998). Each prism is assumed to have constant physical properties, such as density contrast or magnetization. For a rectangular prism with the dimensions limited as $[\xi_1, \xi_2]$, $[\eta_1, \eta_2]$, $[\zeta_1, \zeta_2]$ in the x, y, and z directions (Fig. 1), the vertical component of the gravity attraction Δg and the gravity gradient components at the observation point $P\ (x, y, z_0)$ are given by (Li and Chouteau, 1998; Nagy et al., 2000),

$$\Delta g(x,y,z) = -G\rho \sum_{i=1}^{2}\sum_{j=1}^{2}\sum_{k=1}^{2} u_{ijk}\left[x_i \ln\left(r_{ijk} + y_j\right) + y_j \ln\left(r_{ijk} + x_i\right) - z_k \arctan\frac{x_i y_j}{z_k r_{ijk}}\right], \tag{1}$$

$$V_{zz}(x,y,z) = G\rho \sum_{i=1}^{2}\sum_{j=1}^{2}\sum_{k=1}^{2} u_{ijk} \arctan\frac{x_i y_j}{z_k r_{ijk}}, \tag{2}$$

$$V_{xx}(x,y,z) = G\rho \sum_{i=1}^{2}\sum_{j=1}^{2}\sum_{k=1}^{2} u_{ijk} \arctan\frac{y_j z_k}{x_i r_{ijk}}, \tag{3}$$

$$V_{yy}(x,y,z) = G\rho \sum_{i=1}^{2}\sum_{j=1}^{2}\sum_{k=1}^{2} u_{ijk} \arctan\frac{x_i z_k}{y_j r_{ijk}}, \tag{4}$$

https://doi.org/10.5194/gmd-2022-314
Preprint. Discussion started: 22 March 2023

$$V_{xz}(x,y,z) = -G\rho \sum_{i=1}^{2}\sum_{j=1}^{2}\sum_{k=1}^{2} u_{ijk} \ln\left(r_{ijk} + y_j\right), \tag{5}$$

$$V_{yz}(x,y,z) = -G\rho \sum_{i=1}^{2}\sum_{j=1}^{2}\sum_{k=1}^{2} u_{ijk} \ln\left(r_{ijk} + x_i\right), \tag{6}$$

$$V_{xy}(x,y,z) = -G\rho \sum_{i=1}^{2}\sum_{j=1}^{2}\sum_{k=1}^{2} u_{ijk} \ln\left(r_{ijk} + z_k\right), \tag{7}$$

where G is the universal gravitational constant (6.672×10^{-11} $\mathrm{Nm^2/kg^2}$), ρ is the density contrast of the rectangular prism, $x_i = x - \xi_i$, $y_j = y - \eta_j$, $z_k = z_0 - \zeta_k$, $r_{ijk} = \sqrt{x_i^2 + y_j^2 + z_k^2}$, and $u_{ijk} = (-1)^i(-1)^j(-1)^k$. The z-axis is taken to be positive downward.

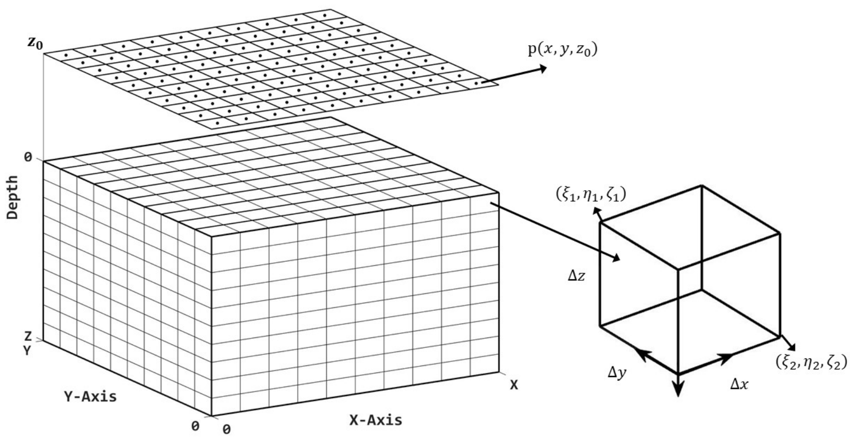

Figure 1: Division schematic diagram of the source region and observation points.

The three components of the magnetic field anomaly (B_x, B_y, B_z) and its gradient tensors due to the prism at the observation point $P(x, y, z_0)$ are given by (Gao, 2019; Luo and Yao, 2007),

$$B_x(x,y,z) = \frac{\mu_0 M}{4\pi} \sum_{i=1}^{2}\sum_{j=1}^{2}\sum_{k=1}^{2} u_{ijk} \left[-k_1 arctan \frac{y_j z_k}{x_i r_{ijk}} + k_2 \ln\left(r_{ijk} + z_k\right) + k_3 \ln\left(r_{ijk} + y_j\right)\right], \tag{8}$$

$$B_y(x,y,z) = \frac{\mu_0 M}{4\pi} \sum_{i=1}^{2}\sum_{j=1}^{2}\sum_{k=1}^{2} u_{ijk} \left[k_1 \ln\left(r_{ijk} + z_k\right) - k_2 arctan \frac{x_i z_k}{y_j r_{ijk}} + k_3 \ln\left(r_{ijk} + x_i\right)\right], \tag{9}$$

https://doi.org/10.5194/gmd-2022-314
Preprint. Discussion started: 22 March 2023

$$B_z(x,y,z) = \frac{\mu_0 M}{4\pi}\sum_{i=1}^{2}\sum_{j=1}^{2}\sum_{k=1}^{2} u_{ijk}\left[k_1 \ln\left(r_{ijk}+y_j\right) + k_2 \ln\left(r_{ijk}+x_i\right) - k_3 arctan\frac{x_i y_j}{z_k r_{ijk}}\right], \quad (10)$$

$$B_{xx}(x,y,z) = -\frac{\mu_0 M}{4\pi}\sum_{i=1}^{2}\sum_{j=1}^{2}\sum_{k=1}^{2} u_{ijk}\left[k_1\frac{y_j z_k\left(r_{ijk}{}^2 + x_i{}^2\right)}{\left(x_i{}^2+z_k{}^2\right)\left(x_i{}^2+y_j{}^2\right)r_{ijk}} + k_2\frac{x_i}{r_{ijk}\left(r_{ijk}+z_k\right)} + k_3\frac{x_i}{r_{ijk}\left(r_{ijk}+y_j\right)}\right], \quad (11)$$

$$B_{yy}(x,y,z) = -\frac{\mu_0 M}{4\pi}\sum_{i=1}^{2}\sum_{j=1}^{2}\sum_{k=1}^{2} u_{ijk}\left[k_1\frac{y_j}{r_{ijk}\left(r_{ijk}+z_k\right)} + k_2\frac{x_i z_k\left(r_{ijk}{}^2 + y_j{}^2\right)}{\left(y_j{}^2+z_k{}^2\right)\left(x_i{}^2+y_j{}^2\right)r_{ijk}} + k_3\frac{y_j}{r_{ijk}\left(r_{ijk}+x_i\right)}\right], \quad (12)$$

$$B_{zz}(x,y,z) = -\frac{\mu_0 M}{4\pi}\sum_{i=1}^{2}\sum_{j=1}^{2}\sum_{k=1}^{2} u_{ijk}\left[k_1\frac{z_k}{r_{ijk}\left(r_{ijk}+y_j\right)} + k_2\frac{z_k}{r_{ijk}\left(r_{ijk}+x_i\right)} + k_3\frac{x_i y_j\left(r_{ijk}{}^2 + z_k{}^2\right)}{\left(x_i{}^2+z_k{}^2\right)\left(y_j{}^2+z_k{}^2\right)r_{ijk}}\right], \quad (13)$$

$$B_{xy}(x,y,z) = B_{yx}(x,y,z) = -\frac{\mu_0 M}{4\pi}\sum_{i=1}^{2}\sum_{j=1}^{2}\sum_{k=1}^{2} u_{ijk}\left[k_1\frac{x_i}{r_{ijk}\left(r_{ijk}+z_k\right)} + k_2\frac{y_j}{r_{ijk}\left(r_{ijk}+z_k\right)} + k_3\frac{1}{r_{ijk}}\right], \quad (14)$$

$$B_{yz}(x,y,z) = B_{zy}(x,y,z) = -\frac{\mu_0 M}{4\pi}\sum_{i=1}^{2}\sum_{j=1}^{2}\sum_{k=1}^{2} u_{ijk}\left[k_1\frac{1}{r_{ijk}} + k_2\frac{y_j}{r_{ijk}\left(r_{ijk}+x_i\right)} + k_3\frac{z_k}{r_{ijk}\left(r_{ijk}+x_i\right)}\right], \quad (15)$$

$$B_{xz}(x,y,z) = B_{zx}(x,y,z) = -\frac{\mu_0 M}{4\pi}\sum_{i=1}^{2}\sum_{j=1}^{2}\sum_{k=1}^{2} u_{ijk}\left[k_1\frac{x_i}{r_{ijk}\left(r_{ijk}+y_j\right)} + k_2\frac{1}{r_{ijk}} + k_3\frac{z_k}{r_{ijk}\left(r_{ijk}+y_j\right)}\right]. \quad (16)$$

where M is the induced magnetization intensity of the rectangular prism with the inclination (I') and declination (D'), $k_1 = cosI'cosD'$, $k_2 = cosI'sinD'$, $k_3 = sinI'$; $\mu_0 = 4\pi\times10^{-7}$ H/m is the magnetic permeability of the vacuum.

Suppose the magnetic anomaly caused by a magnetic body is small compared to the main field. In that case, the scalar magnitude of the magnetic field anomalies can be approximately measured by projecting the components of the anomalous field in the direction of the Earth's main field (Hinze et al., 2013; Plouff, 1976). Therefore, the total magnetic intensity anomaly ΔT and its gradients $(\Delta T_x, \Delta T_x, \Delta T_z)$ of the source can be approximated by (Hinze et al., 2013),

$$\Delta T = B_x cosIcosD + B_y cosIsinD + B_z sinI, \quad (17)$$

$$\Delta T_x = B_{xx} cosIcosD + B_{xy} cosIsinD + B_{zx} sinI, \quad (18)$$

$$\Delta T_y = B_{xy} cosIcosD + B_{yy} cosIsinD + B_{zy} sinI, \quad (19)$$

$$\Delta T_z = B_{xz} cosIcosD + B_{yz} cosIsinD + B_{zz} sinI, \quad (20)$$

where I and D are the inclination and declination of the Earth's geomagnetic field at the observation point.

2.2 Fast forward modelling method

In G&M3D 1.0, we define a source region with the range $[0, X]$, $[0, Y]$, and $[0, Z]$ in the x, y, and z axes, respectively. The source space is divided into $N \times M \times L$ prisms with a size of $\Delta x \times \Delta y \times \Delta z$. The prisms are numbered as (a, b, c), and their dimensions limited are $\left[\xi_{1,a} = (a-1)\Delta x,\ \xi_{2,a} = a\Delta x\right]$, $\left[\eta_{1,b} = (b-1)\Delta y,\ \eta_{2,b} = b\Delta y\right]$, $\left[\zeta_{1,c} = (c-1)\Delta z,\ \zeta_{2,c} = c\Delta z\right]$, where $a = 1,2\ldots,N;\ b = 1,\ldots,M; c = 1,\ldots,L$. As shown in Fig. 1, the observation points (x_n, y_m), where $x_n =$

$(n-0.5)\Delta x, n=1,\dots,N; y_m=(m-0.5)\Delta y,\ m=1,\dots,M$, are distributed at the horizontal surface z_0 on the regular grids aligned with the prism centers.

The above gravity/magnetic fields at the observation $P(x_m, y_n, z_0)$ can be calculated by summing the effects of all the prisms within the source region, which can be written as:

$$\mathrm{g}(x_m, y_n, z_0) = \sum_{c=1}^{L}\left[\sum_{a=1}^{N}\sum_{b=1}^{M} f(a,b,c) \times t(x_n, y_m, z_0; a, b, c)\right], \tag{21}$$

where f is the density or magnetization value corresponding to the prism $(a, \mathrm{b}, \mathrm{c})$, $t(x_m, y_n, z_0; a, b, c)$ is the field response at the observation (x_m, y_n, z_0) due to the prism (a, b, c) with unit density or magnetization, which is calculated by any of Eqs. (1) ~ (16), i.e., the kernel or sensitivity function.

Thanks to Eq. (21), the gravity/magnetic field at all observations can be presented in the matrix-vector form as,

$$\mathbf{g} = \mathbf{K}\cdot \boldsymbol{f} \tag{22}$$

where $\mathbf{g}$ is the field vector, $\boldsymbol{f}$ is the density/magnetic parameter vector, $\mathbf{K}$ represents the kernel matrix (or sensitivity matrix) with dimension (N×M) × (N×M×L), which is a Block-Toeplitz Toeplitz-Block (BTTB) matrix.

The forward calculations in Eq. (22) are time-consuming when the source space is large with a fine discretization. In this study, the 2-D discrete convolution algorithm by block circulant extension (BCE) (Chen and Liu, 2019) is applied to forward calculations of the gravity anomaly, gravity gradient tensors, magnetic components, magnetic gradient tensors, total magnetic intensity, and total magnetic intensity gradients. In G&M3D 1.0, we perform forward calculations of the potential fields by layers along the z direction using the BCE algorithm. The procedure of the BCE algorithm (Chen and Liu, 2019) is as follows. First, the density/magnetization values of all the prisms are stored as a 3-D matrix $\boldsymbol{E}$ with the size $N\times M\times L$. For the c^{th} layer $(c=1,\dots,L)$, the parameter matrix is expressed as $\boldsymbol{f}=\boldsymbol{E}(1{:}N, 1{:}M, c)$. If all elements in the parameter matrix $\boldsymbol{f}$ are zero, it means that all prisms in this layer do not contribute to the observation field, i.e., the effect generated by this layer $\boldsymbol{G}_c = 0$. For other cases, the matrix $\boldsymbol{f}$ is extended by zeros, and we obtain an extended parameter matrix $\mathbf{F}$,

$$\mathbf{F} = \begin{bmatrix} \boldsymbol{f} & \mathbf{0}_{N\times M} \\ \mathbf{0}_{N\times M} & \mathbf{0}_{N\times M} \end{bmatrix}, \tag{23}$$

Secondly, the observation range is extended along the negative direction of the x-axis and y-axis from $[0, X]$, $[0, Y]$ to $[-X+\Delta x, X]$, $[-Y+\Delta y, Y]$, as shown in Fig. 2. The field effects generated by the prism $(a=1, b=1, c)$ (dimensions limited as $[\xi_1=0, \xi_2=\Delta x]$, $[\eta_1=0, \eta_2=\Delta y]$, $[\zeta_1=(c-1)\Delta z,\ \zeta_2=c\Delta z]$) at all the observations in the extended area are computed. We obtain the extended response matrix $\mathbf{T}$ with a size of $(2N-1)\times(2M-1)$ for the c^{th} layer,

$$\mathbf{T} = \begin{bmatrix} t_{1,1} & \cdots & t_{1,2M-1} \\ \vdots & t_{n',m'} & \vdots \\ t_{2N-1,1} & \cdots & t_{2N-1,2M-1} \end{bmatrix} \tag{24}$$

where $t_{n',m'}$ $(n'=1,2,\dots,2N-1; m'=1,2,\dots,2M-1)$ is the field response at the observation $P(x_{n'}, y_{m'}, z_0)$ where $x_{n'}=(n'-N+0.5)\Delta x$, $y_{m'}=(m'-M+0.5)\Delta y$, which is calculated using Eqs. (1) ~ (16) with unit density or induced magnetization intensity (namely, ρ=1, M=1).

https://doi.org/10.5194/gmd-2022-314
Preprint. Discussion started: 22 March 2023

Geoscientific Model Development
Discussions

Extend **T** by zeros along the top and the left margins, as shown in Fig. 2, and construct a matrix $\mathbf{T_0}$ with a size of 2N×2M,

$$\mathbf{T_0} = \begin{bmatrix} 0 & 0_{1\times(2M-1)} \\ 0_{(2N-1)\times 1} & T \end{bmatrix}, \tag{25}$$

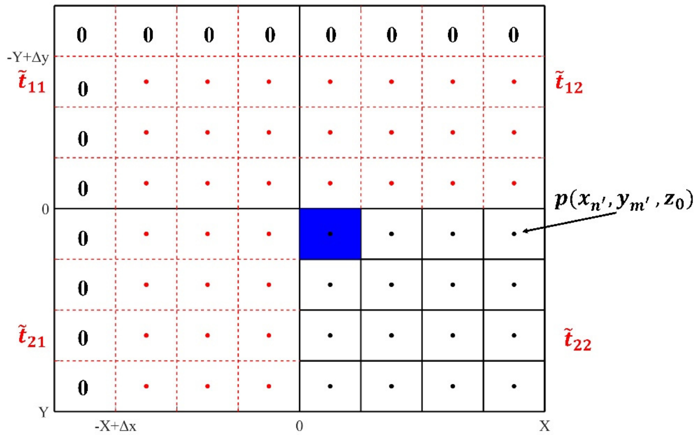

Figure 2: The sketch map shows the extended observation points and source region for the BCE method. The prism (1, 1) is marked in blue color. A single-layer model consisting of 4×4 prisms is taken as an example.

The matrix $\mathbf{T_0}$ in Eq. (25) can be rewritten into four $N \times M$ submatrices as,

$$\mathbf{T_0} = \begin{bmatrix} \tilde{t}_{11} & \tilde{t}_{12} \\ \tilde{t}_{21} & \tilde{t}_{22} \end{bmatrix}, \tag{26}$$

Reorder the submatrices in Eq. (24), we get

$$\mathbf{C} = \begin{bmatrix} \tilde{t}_{22} & \tilde{t}_{21} \\ \tilde{t}_{12} & \tilde{t}_{11} \end{bmatrix}, \tag{27}$$

The matrix **C** in Eq. (27) is a Block-Cyclic-Cyclic-Block (BCCB) matrix. Its 2-D discrete convolution with the extended parameter matrix **F** can be efficiently computed using the fast Fourier transform (Chen and Liu, 2019; Vogel, 2002) as follows,

$$\tilde{\mathbf{C}} = fft2(\mathbf{C}), \tag{28}$$

$$\tilde{\mathbf{F}} = fft2(\mathbf{F}), \tag{29}$$

$$\tilde{\mathbf{G}} = \tilde{\mathbf{C}}.* \tilde{\mathbf{F}}, \tag{30}$$

$$\mathbf{G} = ifft2(\tilde{\mathbf{G}}), \tag{31}$$

$$\mathbf{G}_c = \mathbf{G}(1{:}N, 1{:}M), \tag{32}$$

where $fft2$ is the 2-D fast Fourier transform, and $ifft2$ is the 2-D inverse fast Fourier transform, $.*$ represents dot multiplication operator. $\mathbf{G}_c$ is the resulting field at the observations generated by the anomalous prisms in the c^{th} layer. Repeat the above steps for all layers, and the total field **g** at all observations is obtained by,

https://doi.org/10.5194/gmd-2022-314
Preprint. Discussion started: 22 March 2023

$$\mathbf{g}=\sum_{c=1}^{L}\boldsymbol{G}_c, \tag{33}$$

On the other hand, several additional strategies are applied to increase the efficiency of the BCE method in G&M3D 1.0.

Strategy 1. We take advantage of the fast matrix operation of MATLAB to optimize the forward calculations in G&M3D 1.0. We pre-construct two new matrices $\boldsymbol{X}_i$ and $\boldsymbol{Y}_j$ with the size of $(2N-1)\times(2M-1)$,

$$\boldsymbol{X}_i=\begin{bmatrix} x_1 & \cdots & x_1 \\ \vdots & x_{n'} & \vdots \\ x_{2N-1} & \cdots & x_{2N-1} \end{bmatrix}-\xi_i\mathbf{I}, \tag{34}$$

$$\boldsymbol{Y}_j=\begin{bmatrix} y_1 & \cdots & y_{2M-1} \\ \vdots & y_{m'} & \vdots \\ y_1 & \cdots & y_{2M-1} \end{bmatrix}-\eta_j\mathbf{I}, \tag{35}$$

where i=1, 2; j=1, 2; $x_{n'}=(n'-N+0.5)\Delta x$, $y_{m'}=(m'-M+0.5)\Delta y$, $(n'=1,2,\ldots,2N-1; m'=1,2,\ldots,2M-1)$; $\xi_1=0$, $\xi_2=\Delta x$, $\eta_1=0$, $\eta_2=\Delta y$; $\mathbf{I}$ is the unit matrix with the size of $(2N-1)\times(2M-1)$. Thanks to Eqs. (32)-(33), we substitute the matrices $\boldsymbol{X}_i$ and $\boldsymbol{Y}_j$ to x_i and y_j in any of equations (1)-(16), so the extended response matrix $\mathbf{T}$ at all observations can be computed by a single matrix operation of the dot product in MATLAB instead of a large number of cyclic calculations.

Strategy 2. Since the kernel matrices of gravity components and magnetic components for vertical magnetization are symmetric (Hogue et al., 2020), we only calculate the submatrix $\tilde{\boldsymbol{t}}_{\mathbf{22}}$ in $\mathbf{C}$ (Eq. (25)) for these cases. The other three submatrices ($\tilde{\boldsymbol{t}}_{11}$, $\tilde{\boldsymbol{t}}_{12}$, $\tilde{\boldsymbol{t}}_{21}$) can be obtained by $\tilde{\boldsymbol{t}}_{\mathbf{22}}$, because they are the same or opposite in sign as $\tilde{\boldsymbol{t}}_{\mathbf{22}}$. Therefore, the forward calculations of the gravity anomalies, gravity gradient tensor, and magnetic components with vertical magnetization have a higher efficiency than those of the magnetic field with non-vertical magnetization.

Strategy 3. The variables repeatedly used (e.g., x_i^2, y_j^2, r_{ijk}, ${r_{ijk}}^2$) are stored after the first forward calculation in G&M3D 1.0 and reused in the following calculations. It can reduce the time for the subsequent calculations of other models.

Strategy 4. As we know, the forward calculations of the magnetic fields are related to the declination and inclination of the sources. Suppose the models in the source region have different declinations or inclinations. We classify these models by declinations or inclinations and perform forward calculations of each type separately.

2.3 Synthetic model tests

To verify the efficiency of the forward calculation in G&M3D 1.0, we design a synthetic model with known density and magnetization for the gravity and magnetic forward modeling. The model region ranges from 0 m to 50 km in the x, y, and z axes. The model consists of an anomalous block with a density contrast of 1 g/cm² and induced magnetization of 1 A/m. The center of the anomalous block is located at (25, 25, 25) km with a size of 25×25×20 km. We investigate the computation time for gravity and magnetic forward calculation in cases of three grid numbers, i.e., 100×100×100, 200×200×200, and 500×500×500. Namely, the source region is divided into a combination of prisms with a grid interval of 500 m, 250 m, and 100 m, respectively. The statistics of the absolute computation time for forward computation of the gravity and magnetic fields are presented in Table 1.

https://doi.org/10.5194/gmd-2022-314
Preprint. Discussion started: 22 March 2023

Geoscientific Model Development Discussions
Open Access
EGU

Table 1: The statistics of the absolute consumption time for forward computations of the gravity and magnetic fields with three different grid numbers.

Grid interval (m) / Grid number	Computation time (s)		
	Gravity components	Magnetic components for vertical magnetization	Magnetic components for non-vertical magnetization
500/100×100×100	0.20	0.24	0.67
250/200×200×200	1.55	1.65	7.27
100/500×500×500	27.65	29.48	111.57

Note. All the tests were carried out on a desktop with an i5-12500H CPU and 16 GB memory. No parallel computational strategy is used.

Table 1 presents that the computation time increases significantly with the increase of grid numbers. Note that the output results of the gravity calculation in Table 1 have seven components, i.e., $\Delta g, V_{zz}$, V_{xx}, V_{yy}, V_{xz}, V_{yz}, V_{xy}, and the results of magnetic forward modeling include 13 components (i.e., B_x, B_y, B_z, B_{xx}, B_{yy}, B_{zz}, B_{xy}, B_{xz}, B_{yz}, ΔT, ΔT_x, ΔT_x, ΔT_z). It means that under the three grid numbers, the software G&M3D 1.0 takes only 0.03s, 0.22s, and 3.95s on average, respectively, for calculating each gravity component. For vertical magnetization, it takes 0.02s, 0.13s, and 2.26s on average to compute each component of the magnetic field. It takes 0.51s, 0.56s, and 8.58s on average for non-vertical magnetization. These tests show that G&M3D 1.0 is high-speed for forward calculations of the gravity and magnetic fields. Note that the layers with nonzero density\magnetization occupy 40% of the total layers in the z direction in these tests. The forward calculation will be faster if the anomalous body's vertical dimension is reduced. However, it will take more time when the vertical dimension is more than the present dimension.

3 The framework and functions of G&M3D

In this section, we introduce the functions and operational procedure of G&M3D 1.0. G&M3D 1.0 consists of two main modules: (1) three-dimensional building density or magnetic source models and (2) calculating the gravity or magnetic fields produced by the built source models. The workflow of the G&M3D 1.0 is shown in Fig. 3. When users open G&M3D 1.0 and enter the start interface (Fig. 3), they can open the 3D-Modeling module to create a new source model or input the model data file to conduct the gravity or magnetic forward calculations through the Forward-Modeling module.

The main interface of the Modeling module is shown in Fig. 4. To start constructing a new model, users need to set the source region first by clicking the button “Setting” in the main interface. In the Source-Setting Pop-up window, users can set the basic parameters that define the source region, including the source range, grid interval, and length unit.

https://doi.org/10.5194/gmd-2022-314
Preprint. Discussion started: 22 March 2023

Geoscientific Model Development Discussions
Open Access
EGU

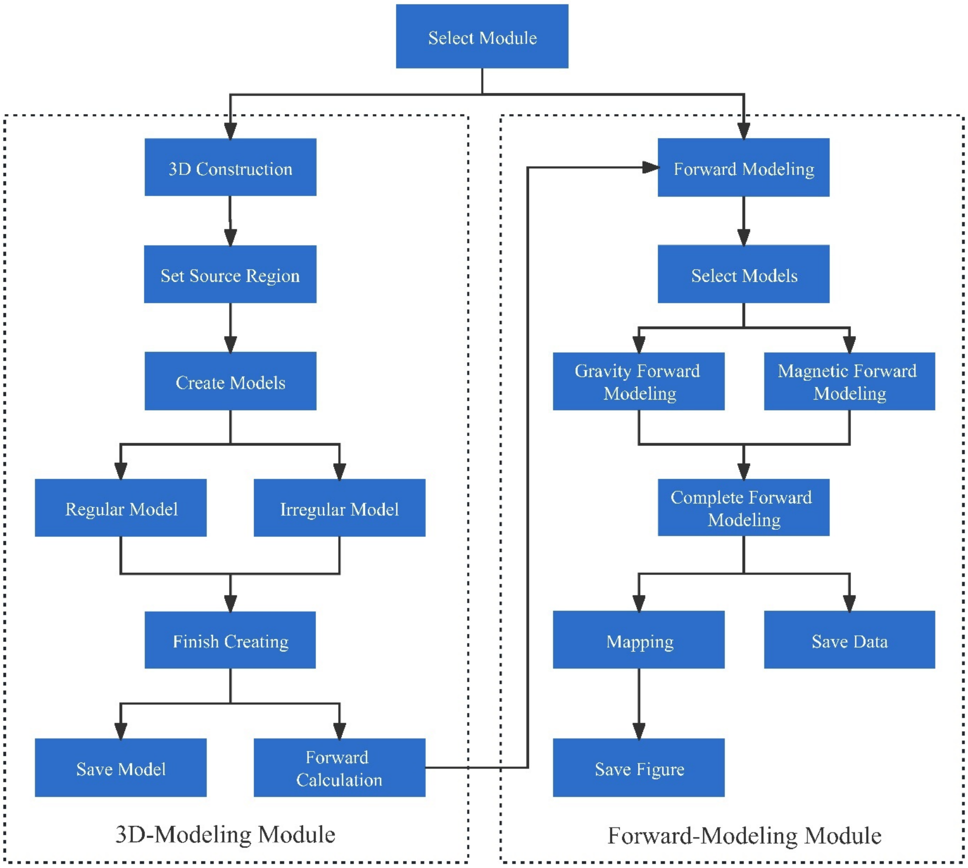

Figure 3: Workflow in G&M3D 1.0.

https://doi.org/10.5194/gmd-2022-314
Preprint. Discussion started: 22 March 2023

Geoscientific Model Development
Discussions
Open Access

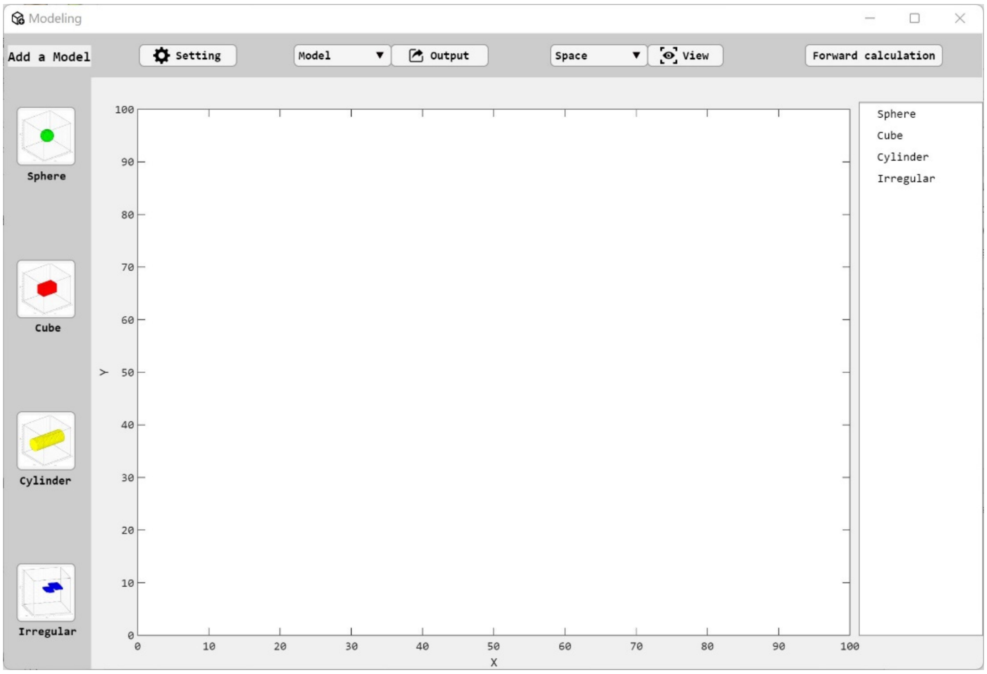

235 **Figure 4: Interface of the Modelling Module. The left side is the model-type option, the middle workspace is used to display the created models, and the list of the models is shown on the right. The button "View" is used to switch the perspective.**

After that, users can select one of the tools on the left of the modeling module interface (Fig. 4) to build a new anomalous body. G&M3D 1.0 provides three tools to build regular bodies, including the **Sphere**, **Cube**, and **Cylinder** tools. Fig. 5 shows the parameter input interfaces for the three tools. On the other hand, G&M3D 1.0 provides the **Irregular** tool to create irregular models, as shown in Fig. 6. Using the **Irregular** tool, users can construct irregularly shaped bodies by drawing their boundaries layer by layer. G&M3D 1.0 automatically generates a set of prisms to fit the limits that users draw in one layer along the x, y, or z direction. Accordingly, G&M3D 1.0 provides three drawing modes: **rectangle**, **circle**, and **freehand**. In the **freehand** mode, users can draw any closed curve to define the boundary of the anomalous body. The automatically formed prisms fit the limits more accurately with gradual sketching. If the automatically generated shape cannot meet the demand, G&M3D 1.0 also provides the **Single Point** mode to add or delete a cell for patching.

https://doi.org/10.5194/gmd-2022-314
Preprint. Discussion started: 22 March 2023

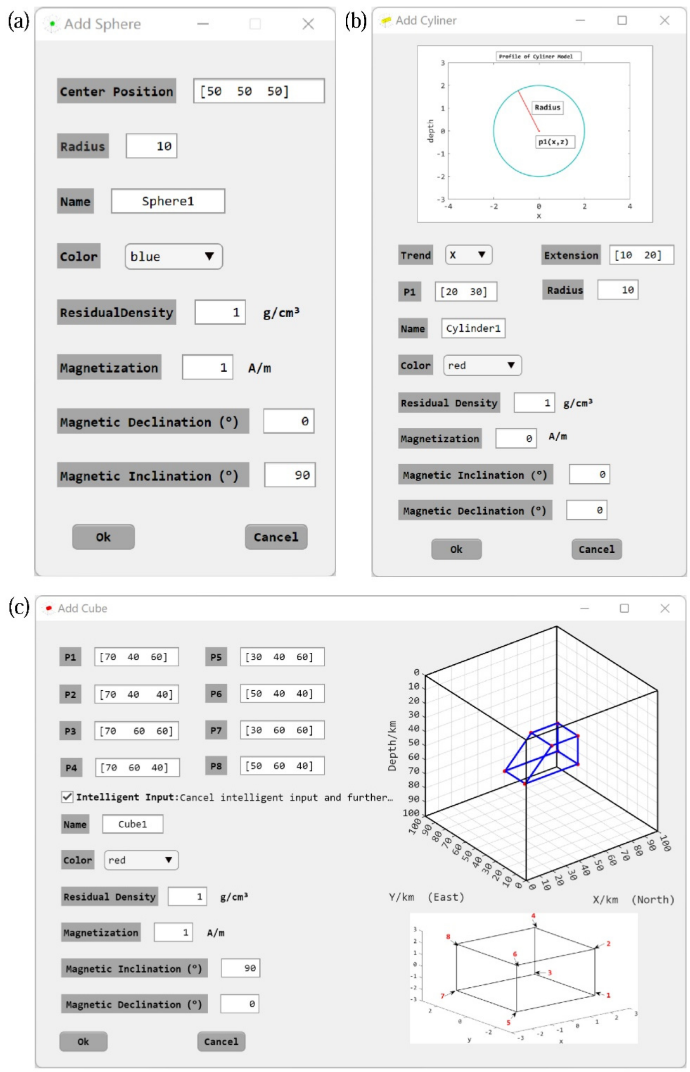

Figure 5: Parameter input interfaces for the three regular tools, including (a) Sphere, (b) Cylinder, and (c) Cube. For the Sphere tool, the radius and centre of the sphere are necessary. The Cylinder tool requires the trend direction, extension length, and section centre. The Cube tool needs the coordinates for the cube's eight corners. All models require the input of density contrast or magnetization. Users can also set the name and colour of the model independently.

https://doi.org/10.5194/gmd-2022-314
Preprint. Discussion started: 22 March 2023

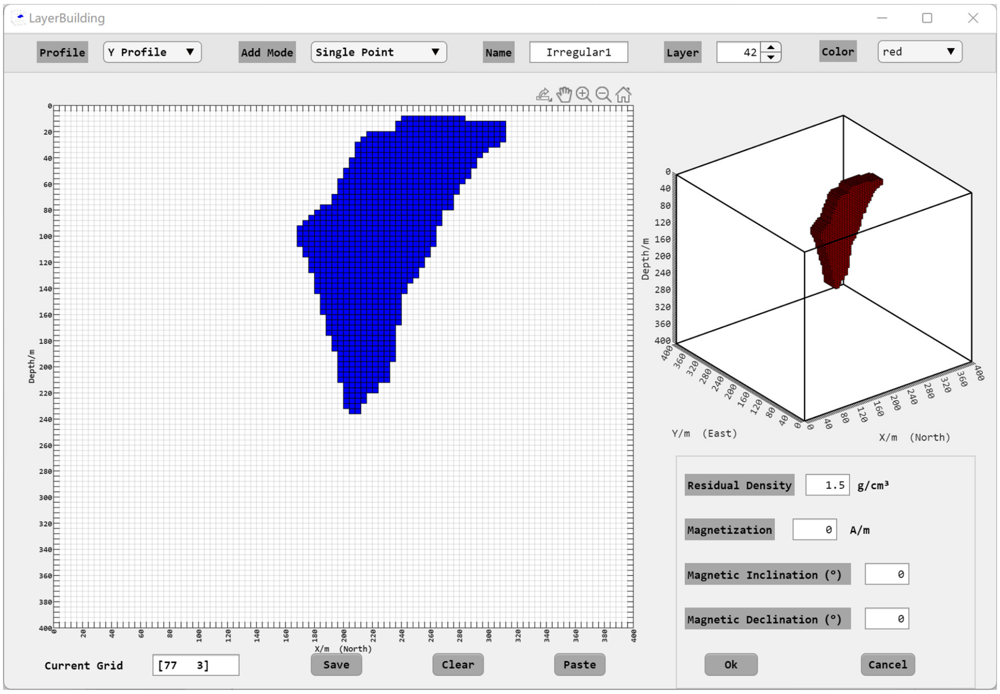

Figure 6: Interface of the Irregular tool. The left-middle workspace is used to draw the boundaries of the anomalous body. The right-upper area is used to display a 3D drawing of the model. Button Save and Clear are used to save and clear the prisms of the current layer. Button Paste is used to copy the previous layer's prisms to the current layer. A sulphide deposit with a density contrast of 1.5 g/cm^3 is an example, adapted according to Thomas (1997).

After all the models are created, the model data and the spatial distribution of the density/magnetization within the source region can be exported. Users can also directly import the created models into the Forward-Modeling module for forward calculation. Fig. 7 shows the main interface of the Forward-Modeling module.

To perform forward calculations, users first need to set the observation parameters through the GRA-FWD and MAG-FWD interface, as shown in Fig. 8. Subsequently, users can carry out the forward calculation by clicking the **Gravity Forward** or **Magnetic Forward** buttons. After the forward analysis is completed, G&M3D 1.0 automatically draws the contour map of the results. Users can switch to other data using the drop-down box in the Forward-Modeling interface. The source model and its field are also visualized in the same coordinate system, which is helpful for data analysis. In addition, users can view the gravity or magnetic field along profiles using the right-lower workspace. The forward modeling results can be viewed in G&M3D 1.0 or exported as a dataset by clicking the button "**Data**". The button "**Draw**" is used to format the drawing.

https://doi.org/10.5194/gmd-2022-314
Preprint. Discussion started: 22 March 2023

Geoscientific Model Development
Open Access
EGU
Discussions

(a)

(b)

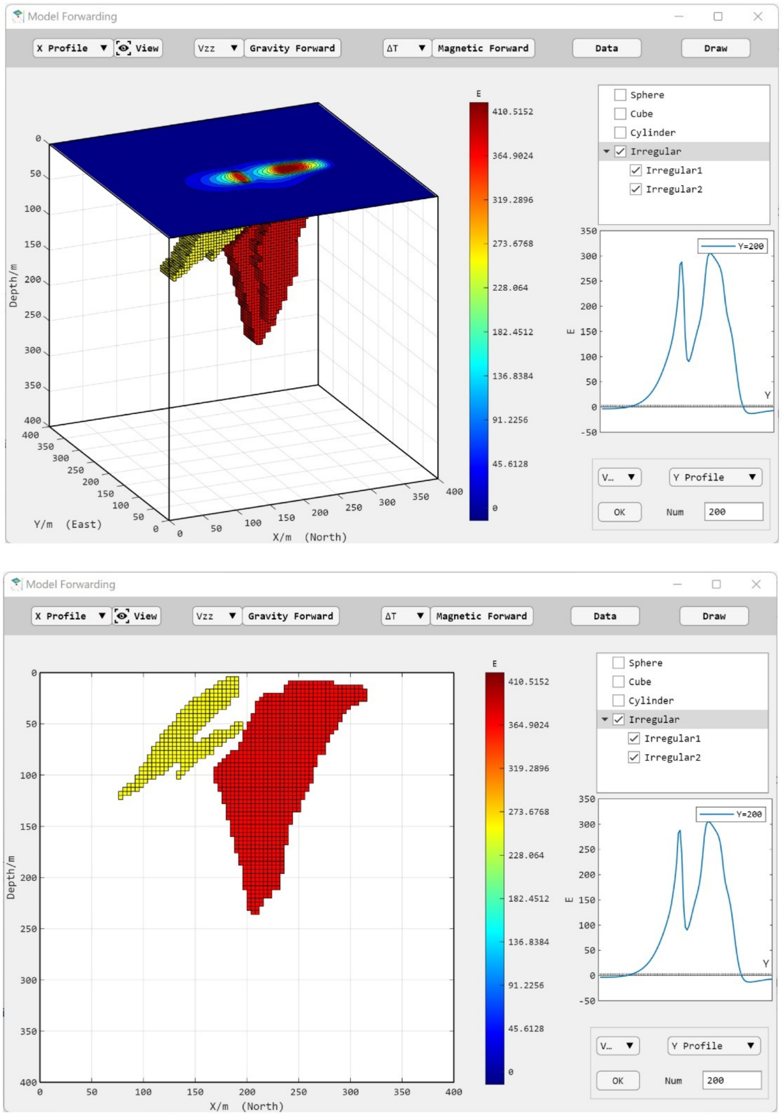

Figure 7: Interface of Forward-Modelling module in (a) 3D view, (b) 2D view along the X profile. The left-middle workspace is used to visualize the model and its gravity/magnetic field. The upper right area shows the model list, and different models can be selected for forward calculation. The right lower area exhibits the vertical gravity gradient **anomalies along a profile. A sulphide deposit is shown as an example, which is adapted according to Thomas (1997).**

https://doi.org/10.5194/gmd-2022-314
Preprint. Discussion started: 22 March 2023

Geoscientific Model Development Discussions
Open Access

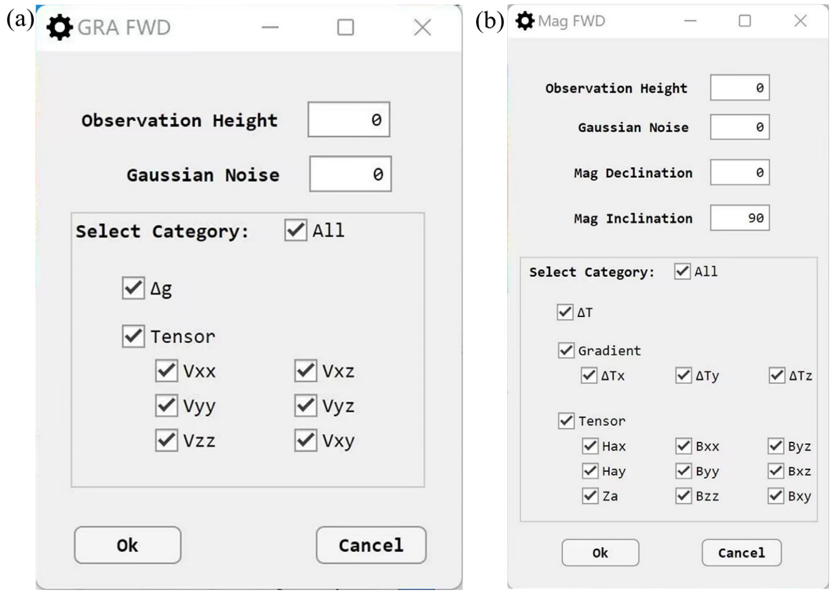

Figure 8: Parameter input pop-up window for (a) Gravity forward modeling (b) Magnetic forward modeling. A certain proportion of Gaussian noises can be added to the field values to simulate errors. Mag-Inclination and Mag-Declination correspond to the inclination (*I*), and declination (*D*) of the Earth's geomagnetic field in Eqs. (17)-(20). Users can freely select the field category to be calculated.

4 Application

The 3D modeling and forward calculations of the gravity and magnetic fields in G&M3D 1.0 provide practical tools for potential data analysis and interpretation. It also can assist the research on the forward and inversion algorithm of gravity and magnetic data. Researchers usually need to conduct synthetic model experiments to verify algorithm feasibility and parameter sensitivity. Using G&M3D 1.0, researchers can easily create a large number of artificial density or susceptibility models and quickly obtain the gravity/magnetic fields generated by these models. In addition, G&M3D 1.0 can also be used in geophysical teaching, especially for students new to gravity and magnetic exploration. Teachers and students can create simple geophysical models and analyze the principles of the potential field by using G&M3D 1.0.

To illustrate the usage of G&M3D 1.0, we carry out the gravity modeling of a distinctive salt dome as an example. This salt dome model was constructed based on available seismic and drill-hole data in Vinton Dome, southern Louisiana (Ennen, 2012). It comprises a positive-density caprock at the depths 160 ~ 760 m and a negative-density salt volume at deep depths. Ennen (2012) calculated the gravity gradients produced by this salt dome model and compared them with the observed airborne

https://doi.org/10.5194/gmd-2022-314
Preprint. Discussion started: 22 March 2023

gravity gradient data to explore potential oil signals. As presented in the study by Ennen (2012), building this irregular salt dome density model is tedious.

Here we use this salt dome model (Ennen, 2012) as an example to illustrate the 3-D modeling and forward calculations of the gravity gradients by G&M3D 1.0. According to Ennen (2012), the source space is divided into 66 × 45 × 28 prisms with a size of 100 × 100 × 100 m. The density anomaly salt dome has different geometry at the depth with varying density contrasts, as presented in Table 2.

Table 2: Density distribution of the salt dome model along the depth

Anomalous body number	Depth range of sources /m	Density contrast (kg/m^3)
1	60-160	575
2	160-260	575
3	260-360	400
4	360-460	400
5	460-760	50
6	760-1060	-20
7	1060-1360	-50
8	1360-1660	-70
9	1660-1960	-100
10	1960-2260	-130
11	2260-2560	-150
12	2560-2860	-170

In G&M3D 1.0, we apply the **Irregular** tool in the Modeling Module to build this salt dome model. According to its density distribution, this salt dome structure can be approximated by 12 separate irregular bodies at different depths, with each body having a constant density (Table 2). We build them successively using the Modeling Module in G&M3D 1.0. In the Modeling Module, we first set the source region range with [0 70], [0 70], and [0 50] in the x, y, and z axes, respectively, with the unit hm (hundred meters). The division step is set to be 1×1×1 hm. Subsequently, in the Layer-Building interface, we specify the layer number to be 28 and the density contrast to be -170 kg/m^3. Using the **freehand** mode, we delineate the geometry of the salt dome at this depth on the workspace and then use the **Single Point** mode to modify its shape slightly. After the modification, we save this anomalous body and change the layer number to 27. At this time, the source geometry on the previous layer is portrayed on the interface to assist us in locating the anomaly source. We can also directly copy and paste the body from the last layer. This can be done repeatedly to build the salt dome model quickly (Fig. 9).

https://doi.org/10.5194/gmd-2022-314
Preprint. Discussion started: 22 March 2023

Geoscientific Model Development
Discussions
Open Access
EGU

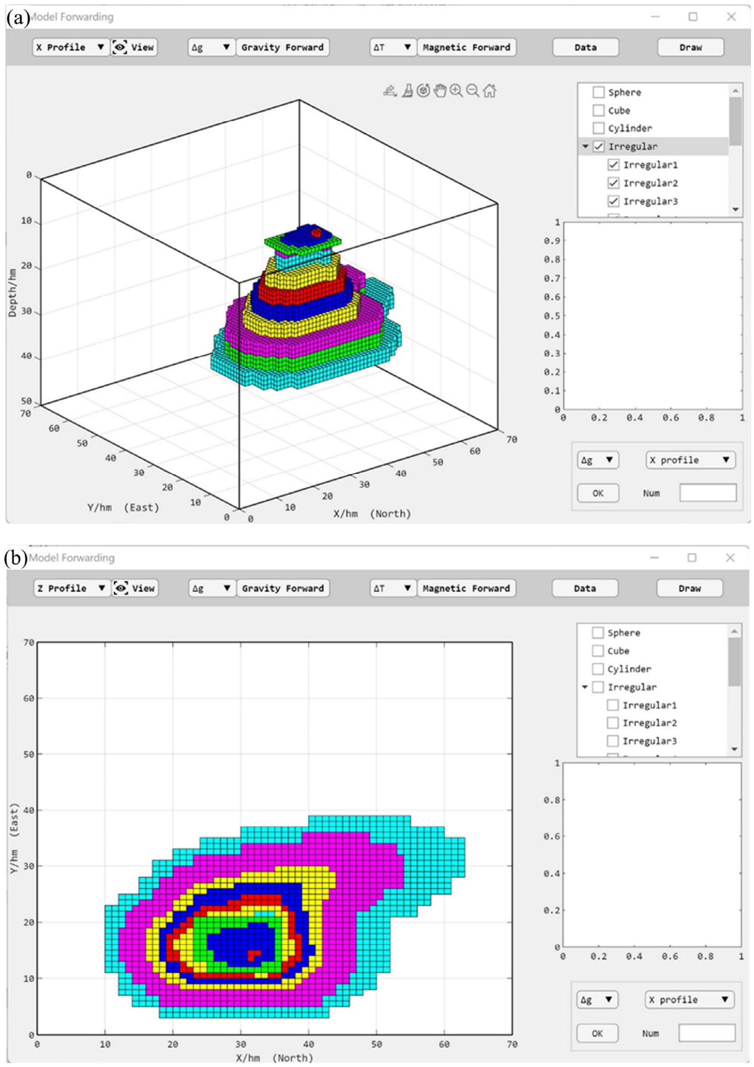

Figure 9: The salt dome model built by G&M3D 1.0. (a) 3D view, (b) 2D view along the z profile in the workspace.

After the 12 anomalous bodies that make up the salt dome model are constructed, we use the Forward Modeling Module to determine its gravity gradients. We set the observation range as the same as the source. The observation height is set to be 0 m. The obtained gravity gradient components are shown in Fig. 10. The data are consistent with the forward simulation data

https://doi.org/10.5194/gmd-2022-314
Preprint. Discussion started: 22 March 2023

given by Ennen (2012), proving the validity of the forward calculation in G&M3D. The convenient 3D modeling, forward computation, and visualization process also demonstrate the practicality of G&M3D.

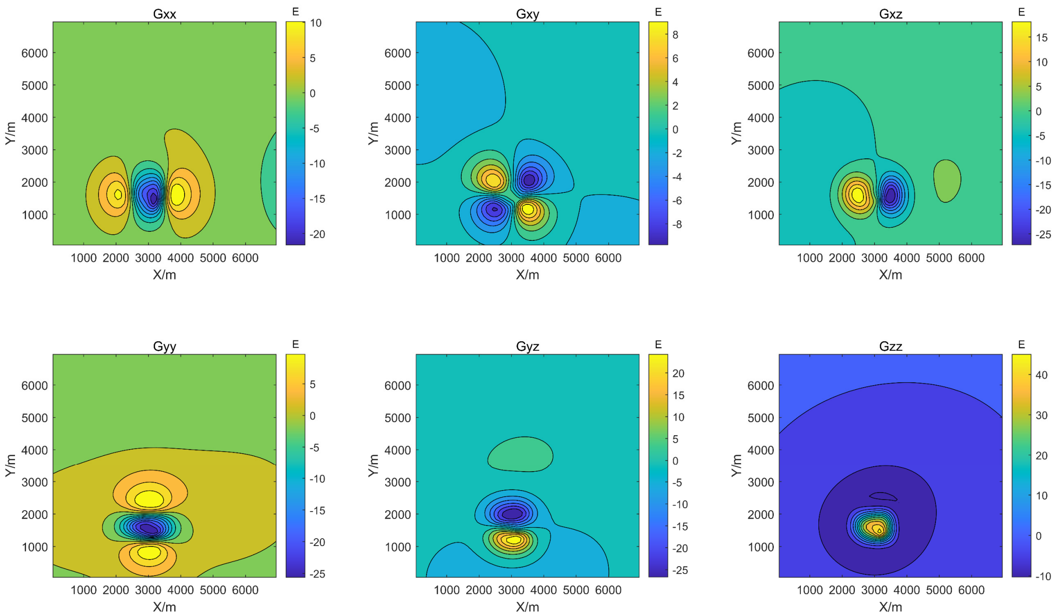

Figure 10: The gravity gradient components generated by the salt dome model using G&M3D 1.0.

5 Conclusions

The study developed an open-source software — G&M3D 1.0, based on the MATLAB app designer platform. G&M3D 1.0 was developed to construct 3D models of density and magnetization and compute their gravity and magnetic fields. The software can be used as independent desktop software or as a MATLAB built-in plug-in. Using G&M3D 1.0, users can easily create arbitrary source models, and achieve model modification, deletion, storage, and display. Furthermore, we expanded the efficient BCE algorithm to forward calculations of the gravity gradient tensors and magnetic gradient tensors. Finally, we presented the gravity modeling over the Vinton salt dome in southern Louisiana, U.S. The practical application shows how G&M3D 1.0 may be applied to geophysical research, training, and data processing and interpretation.

Code availability

The software and data involved in this paper have been open source and uploaded to Zendo community.

Name of the code/library: G&M3D 1.0

Contact: bochen@csu.edu.cn, weikanggui22@mails.ucas.ac.cn

Hardware requirements: Running memory is greater than 3G

Program language: MATLAB

Software required: MATLAB 2018a or above

Program size: 4.2MB

The source codes are available for download at the link: https://doi.org/10.5281/zenodo.7752086.

Author contribution

Kanggui Wei: Developed the MATLAB codes, Drafted the paper. **Bo Chen:** Provided the ideas and their implementation and revised the paper. **Jiaxiang Peng:** Provided the initial functions for magnetic forward calculations.

Competing interests

The authors declare that they have no conflict of interest.

Acknowledgments

We thank Xiaomin Zuo for her support and help in software programming and writing. We thank Longwei Chen, Siyang Li and Shiyu Zhang for their help in the software development. We thank the High-Performance Computing Center of Central South University for support. The research is supported by the National Natural Science Foundation of China (Grant No. 42074109).

References

Battaglia, M., Calahorrano-Di Patre, A., Flinders, A.F., 2022. gTOOLS, an open-source MATLAB program for processing high precision relative gravity data for time-lapse gravity monitoring. Computers & Geosciences 160.

Bhattacharyya, B., 1964. Magnetic anomalies due to prism-shaped bodies with arbitrary polarization. Geophysics 29, 517-531.

Bhattacharyya, B., Navolio, M., 1976. A fast Fourier transform method for rapid computation of gravity and magnetic anomalies due to arbitrary bodies. Geophys. Prospect. 24, 633-649.

Blakely, R.J., 1996. Potential theory in gravity and magnetic applications. Cambridge university press.

Caratori Tontini, F., Cocchi, L., Carmisciano, C., 2009. Rapid 3-D forward model of potential fields with application to the Palinuro Seamount magnetic anomaly (southern Tyrrhenian Sea, Italy). J. Geophys. Res. 114.

Chen, L., Liu, L., 2019. Fast and accurate forward modelling of gravity field using prismatic grids. Geophys. J. Int. 216, 1062-1071.

de la Varga, M., Schaaf, A., Wellmann, F., 2019. GemPy 1.0: open-source stochastic geological modeling and inversion. Geoscientific Model Development 12, 1-32.

Ennen, C., 2012. Mapping gas-charged fault blocks around the Vinton Salt Dome, Louisiana using gravity gradiometry data.

Gao, X., 2019. The study and application of 3D inversion methods of gravity & magnetic and their gradient tensor data [Ph. D. thesis]. Changchun: Jilin University.

Guo, Z.H., Guan, Z.N., Xiong, S.Q., 2004. Cuboid Delta T and its gradient forward theoretical expressions without analytic odd points. Chinese Journal of Geophysics-Chinese Edition 47, 1131-1138.

Hassanzadeh, A., Vázquez-Suñé, E., Corbella, M., Criollo, R., 2022. An automatic geological 3D cross-section generator: Geopropy, an open-source library. Environmental Modelling & Software 149, 105309.

Hinze, W.J., von Frese, R.R.B., Saad, A.H., 2013. Gravity and magnetic exploration: Principles, practices, and applications. Cambridge University Press.

Hogue, J.D., Renaut, R.A., Vatankhah, S., 2020. A tutorial and open source software for the efficient evaluation of gravity and magnetic kernels. Computers & Geosciences 144, 104575.

Jessell, M., Aillères, L., De Kemp, E., Lindsay, M., Wellmann, F., Hillier, M., Laurent, G., Carmichael, T., Martin, R., 2014. Next generation three-dimensional geologic modeling and inversion.

Jessell, M., Ogarko, V., De Rose, Y., Lindsay, M., Joshi, R., Piechocka, A., Grose, L., De La Varga, M., Ailleres, L., Pirot, G., 2021. Automated geological map deconstruction for 3D model construction using map2loop 1.0 and map2model 1.0. Geoscientific Model Development 14, 5063-5092.

Li, X., Chouteau, M., 1998. Three-dimensional gravity modeling in all space. Surv. Geophys. 19, 339-368.

Luo, Y., Yao, C., 2007. Forward modeling of gravity, gravity gradients, and magnetic anomalies due to complex bodies. Journal of China University of Geosciences 18, 280-286.

Nagy, D., 1966. The gravitational attraction of a right rectangular prism. Geophysics 31, 362-371.

Nagy, D., Papp, G., Benedek, J., 2000. The gravitational potential and its derivatives for the prism. J. Geod. 74, 552-560.

Okabe, M., 1979. Analytical expressions for gravity anomalies due to homogeneous polyhedral bodies and translations into magnetic anomalies. Geophysics 44, 730-741.

Özgü Arısoy, M., Dikmen, Ü., 2011. Potensoft: MATLAB-based software for potential field data processing, modeling and mapping. Computers & Geosciences 37, 935-942.

Pallero, J.L.G., Fernández-Martínez, J.L., Fernández-Muñiz, Z., Bonvalot, S., Gabalda, G., Nalpas, T., 2021. GravPSO2D: A Matlab package for 2D gravity inversion in sedimentary basins using the Particle Swarm Optimization algorithm. Computers & Geosciences 146.

Pham, L.T., Oksum, E., Gómez-Ortiz, D., Do, T.D., 2020. MagB_inv: A high performance Matlab program for estimating the magnetic basement relief by inverting magnetic anomalies. Computers & Geosciences 134.

Pirot, G., Joshi, R., Giraud, J., Lindsay, M.D., Jessell, M.W., 2022. loopUI-0.1: indicators to support needs and practices in 3D geological modelling uncertainty quantification. Geoscientific Model Development 15, 4689-4708.

Plouff, D., 1976. Gravity and magnetic fields of polygonal prisms and application to magnetic terrain corrections. Geophysics 41, 727-741.

Qiang, J., Zhang, W., Lu, K., Chen, L., Zhu, Y., Hu, S., Mao, X., 2019. A fast forward algorithm for three-dimensional magnetic anomaly on undulating terrain. J. Appl. Geophys. 166, 33-41.

Stocco, S., Godio, A., Sambuelli, L., 2009. Modelling and compact inversion of magnetic data: A Matlab code. Computers & Geosciences 35, 2111-2118.

Thomas, M., 1997. Gravity Prospecting For Massive Sulphide Deposits in the Bathurst Mining Camp, New Brunswick, Canada, pp. 837-840.

Vogel, C.R., 2002. Computational methods for inverse problems. SIAM.

Wellmann, J.F., Thiele, S.T., Lindsay, M.D., Jessell, M.W., 2016. pynoddy 1.0: an experimental platform for automated 3-D kinematic and potential field modelling. Geoscientific Model Development 9, 1019-1035.

Wu, L.Y., Tian, G., 2014. High-precision Fourier forward modeling of potential fields. Geophysics 79, G59-G68.

Yuan, Y., Cui, Y., Chen, B., Zhao, G., Liu, J., Guo, R., 2022. Fast and high accuracy 3D magnetic anomaly forward modeling based on BTTB matrix. Chinese Journal of Geophysics-Chinese Edition 65, 1107-1124.

Zhang, Y., Wong, Y.S., 2015. BTTB-based numerical schemes for three-dimensional gravity field inversion. Geophys. J. Int. 203, 243-256.

Zhao, G., Chen, B., Chen, L., Liu, J., Ren, Z., 2018. High-accuracy 3D Fourier forward modeling of gravity field based on the Gauss-FFT technique. J. Appl. Geophys. 150, 294-303.